

1 **Atmospheric changes caused by galactic cosmic rays over**
2 **the period 1960-2010**

3

4 **Charles H. Jackman¹, Daniel R. Marsh², Douglas E. Kinnison², Christopher J.**
5 **Mertens³, and Eric L. Fleming^{4,5}**

6 [1](Emeritus, NASA Goddard Space Flight Center, Greenbelt, MD, U.S.A.)

7 [2](National Center for Atmospheric Research, Boulder, CO, U.S.A.)

8 [3](NASA Langley Research Center, Hampton, VA, U.S.A.)

9 [4](NASA Goddard Space Flight Center, Greenbelt, MD, U.S.A.)

10 [5](Also at Science Systems and Applications, Inc., Lanham, MD, U.S.A.)

11 Correspondence to: Charles H. Jackman (Charles.H.Jackman@nasa.gov)

12

1 **Abstract**

2 The Specified Dynamics version of the Whole Atmosphere Community Climate Model (SD-
3 WACCM) and the Goddard Space Flight Center two-dimensional (GSFC 2-D) models are
4 used to investigate the effect of galactic cosmic rays (GCRs) on the atmosphere over the
5 1960-2010 time period. The Nowcast of Atmospheric Ionizing Radiation for Aviation Safety
6 (NAIRAS) computation of the GCR-caused ionization rates are used in these simulations.

7 GCR-caused maximum NO_x increases of 4-15% are computed in the Southern polar
8 troposphere with associated ozone increases of 1-2%. NO_x increases of ~1-6% are calculated
9 for the lower stratosphere with associated ozone decreases of 0.2-1%. The primary impact of
10 GCRs on ozone was due to their production of NO_x. The impact of GCRs varies with the
11 atmospheric chlorine loading, sulfate aerosol loading, and solar cycle variation. Because of
12 the interference between the NO_x and ClO_x ozone loss cycles (e.g., the ClO + NO₂ + M →
13 ClONO₂ + M reaction) and the change in the importance of ClO_x in the ozone budget, GCRs
14 cause larger atmospheric impacts with less chlorine loading. GCRs also cause larger
15 atmospheric impacts with less sulfate aerosol loading and for years closer to solar minimum.
16 GCR-caused decreases of annual average global total ozone (AAGTO) were computed to be
17 0.2% or less with GCR-caused tropospheric column ozone increases of 0.08% or less and
18 GCR-caused stratospheric column ozone decreases of 0.23% or less. Although these
19 computed ozone impacts are small, GCRs provide a natural influence on ozone and need to be
20 quantified over long time periods.

1 **1 Introduction**

2 Galactic cosmic rays (GCRs) from outside the solar system are comprised of highly energetic
3 charged particles and are believed to be the result of supernovae events and other high energy
4 astrophysical processes. GCRs contain a wide range of energetic particles, which are also
5 influenced by the Earth's magnetosphere. High energy GCRs not only penetrate further into
6 the atmosphere, but can also cause atmospheric effects outside the polar cap regions. The
7 flux of GCRs is larger during solar minimum, when the reduced solar magnetic field less
8 effectively shields the solar system from the particles.

9 The influence of galactic cosmic rays (GCRs) on the middle atmosphere has been studied
10 since the 1970's (e.g., Warneck 1972; Ruderman and Chamberlain, 1975; Nicolet 1975;
11 Jackman et al., 1980, 1987, 1996; Thorne 1980; Garcia et al., 1984; Legrand et al., 1989;
12 Jackman 1991, 1993; Müller and Crutzen, 1993; Vitt and Jackman, 1996; Krivolutsky et al.,
13 1999, 2001, 2002; Vitt et al., 2000; Semeniuk et al., 2011; Calisto et al., 2011). These
14 previous studies made use of GCR-produced ionization rates (GPIR) in computing
15 atmospheric chemistry impacts. The GPIR were deduced primarily in a couple of different
16 methodologies.

17 For example, Nicolet (1975) made use of balloon soundings and ionization chambers to
18 compute the GPIR. Several of the other earlier studies roughly followed the Nicolet (1975)
19 methodology for inclusion of GPIR in atmospheric analyses. A more recent study by Calisto
20 et al. (2011) primarily relied on the computations of the Cosmic Ray induced Cascade:
21 Application for Cosmic Ray Induced Ionization (CRAC:CRII) of Usoskin et al. (2010) to
22 deduce the GPIR. Another method of computing GPIR has been developed by the Nowcast of
23 Atmospheric Ionizing Radiation for Aviation Safety (NAIRAS) team at NASA Langley
24 Research Center (see Mertens et al., 2013). The NAIRAS-deduced GPIR has been computed
25 over the years 1960-2010. The solar cycle shows substantial variation over this 51-year time
26 period, which is reflected in the GPIR.

27 GCRs also affect the atmosphere through the production of the important constituent families
28 of NO_x (N, NO, NO_2) and HO_x (H, OH, HO_2) either directly or through a photochemical
29 sequence. The NAIRAS-deduced GPIR and subsequent NO_x and HO_x production can be used
30 in atmospheric models to predict impact on constituents over the 1960-2010 period. We use
31 two models, the Specified Dynamics – Whole Atmosphere Community Climate Model (SD-
32 WACCM) and the Goddard Space Flight Center (GSFC) two-dimensional (2-D) model, to

1 study the influence of GCRs on the atmosphere over these 51 years. SD-WACCM is used for
2 detailed studies of the impact of GCRs on minor atmospheric constituents. The GSFC 2-D
3 model helps in the quantification of the changing GCR influence between 1960 and 2010 as
4 the chlorine-loading, sulfate aerosol amount, solar cycle, and dynamics vary over this time
5 period. The fast computational speed of the GSFC 2-D model (compared with SD-WACCM)
6 allows a number of simulations to investigate the sensitivity of the GCR influence in different
7 changing background atmospheres.

8 This paper is divided into six primary sections, including the Introduction. The NAIRAS
9 GCR ionization rate computation is discussed in Section 2 and the GCR-induced production
10 of HO_x and NO_x are discussed in Section 3. A description of the two models (SD-WACCM
11 and GSFC 2-D) used in this work are given in Section 4. Model results (both SD-WACCM
12 and GSFC 2-D) for several GCR-caused atmospheric constituent changes are shown in
13 Section 5. The conclusions are presented in Section 6.

14 **2 NAIRAS GCR ionization rate**

15 The Nowcast of Atmospheric Ionizing Radiation for Aviation Safety (NAIRAS) team at
16 NASA Langley Research Center (see <http://sol.spacenvironment.net/~nairas/>) has developed
17 and integrated a model to include GCRs into their ionizing radiation computation. The
18 interplanetary magnetic field varies over a solar cycle and provides a modulation of the GCR
19 spectral flux, which has been referred to as a solar modulation potential (e.g., Badhwar and
20 O'Neill, 1996). For real-time application of the NAIRAS model, four real-time, high-latitude,
21 ground-based neutron monitor count rate measurements are used to cross correlate with the
22 solar modulation potential and provide the NAIRAS model's GCR spectral flux incident on
23 the Earth for penetration into and through the atmosphere. NAIRAS is a physics-based model
24 that maximizes the use of measurement input data (Mertens et al., 2013, and references
25 therein).

26 In the NAIRAS model, GCRs travel from outside the heliosphere to 1 AU by the Badhwar
27 and O'Neill (1992, 1994, 1996) and O'Neill (2010) NASA model, with the solar modulation
28 potential determined from measurements of ground-based neutron monitor count rates. The
29 GCR spectral flux at 1 AU travel through the magnetosphere by means of a transmission
30 factor determined by the vertical geomagnetic cutoff rigidity computed in the International
31 Geomagnetic Reference Field model (Finlay et al., 2010). The vertical cutoff rigidities are
32 determined by numerical solutions of charged particle trajectories in the IGRF field using the

1 techniques advanced by Smart and Shea (1994, 2005). After transmission through the
2 magnetosphere, the GCR spectral flux travels through the neutral atmosphere using the
3 NASA HZETRN deterministic transport code (Mertens et al., 2012). The global distribution
4 of atmospheric mass density is obtained from NCAR/NCEP Reanalysis 1 data at pressure
5 levels larger than 10 hPa (Kalnay et al., 1996) and the Naval Research Laboratory Mass
6 Spectrometer and Incoherent Scatter model atmosphere data at pressure levels less than 10
7 hPa (Picone et al., 2002).

8 The NAIRAS model has been used to compute the annual average GCR-produced ionization
9 rates (GPIR) for the 1960-2010 time periods. For these time periods, measurements from the
10 Thule and Izmiran neutron monitor stations were used to determine the solar modulation
11 potential. GPIR in the NAIRAS model are computed by multiplying the dose rate in air by the
12 atmospheric density, divided by 35 eV per ion-pair. The annual average GPIR from the
13 NAIRAS model for two years, 2002 and 2009, are presented in Figure 1. This shows the
14 inverse relationship between GPIR and solar activity. Year 2002 is very close to solar
15 maximum and shows a smaller GPIR with maximum ionization rates of nearly $15 \text{ cm}^{-3} \text{ s}^{-1}$,
16 whereas year 2009 is very close to solar minimum with about a factor of two larger maximum
17 ionization rate of $30 \text{ cm}^{-3} \text{ s}^{-1}$. The time-dependent variation in the GPIR at 90°S and 90°N is
18 given in Figure 2. Peaks in GPIR occur in 1965, 1977, 1987, 1997, and 2009, reflective of
19 solar minimum conditions in those years. The North-South asymmetry in the GPIR is due to a
20 systematic hemispherical asymmetry in the NCEP atmospheric density profiles.

21 The Mertens et al. (2013) GPIR are about a factor of two smaller than those presented in
22 Usoskin et al. (2010), and the altitude of the maximum in the GPIR is lower in the NAIRAS
23 results as well. A comparison of these two computations of GCR ion rates at 90 degrees N is
24 given in Figure 3 for both solar minimum (1965) and solar maximum (1960) conditions. The
25 underprediction of the NAIRAS GPIR and the lower altitude of its maximum is due to the
26 lack of pion-initiated electromagnetic cascade processes in the HZETRN version 2010
27 currently implemented in the NAIRAS model (Mertens et al., 2013). This deficiency will
28 soon be rectified when the 2015 version of HZETRN is integrated into the NAIRAS model
29 (e.g., Norman et al., 2012, 2013; Slaba et al. 2013).

30 **3 NO_x (N, NO, NO₂) and HO_x (H, OH, HO₂) production**

31 Besides ionization, GCRs also produce the important constituent families of NO_x (N, NO,
32 NO₂) and HO_x (H, OH, HO₂) either directly or through a photochemical sequence. NO_x is

1 produced when the cosmic rays (primarily protons and their associated secondary electrons)
2 dissociate N₂ as they precipitate into the atmosphere. Here it is assumed that 1.25 N atoms
3 are produced per ion pair and the proton impact of N atom production is divided between the
4 ground state N(⁴S) (45% or 0.55 per ion pair) and excited state N(²D) (55% or 0.7 per ion
5 pair) nitrogen atoms (Porter et al., 1976). GCRs also result in the production of HO_x through
6 complex positive ion chemistry (Solomon et al., 1981). The charged particle-produced HO_x is
7 a function of ion pair production and altitude and is included in model simulations using a
8 lookup table from Jackman et al. (2005, Table 1), which is based on the work of Solomon et
9 al. (1981). Each ion pair results in the production of about two HO_x constituents for the
10 troposphere, stratosphere, and lower mesosphere and less than two HO_x constituents for the
11 middle and upper mesosphere.

12 **4 Model Predictions**

13 **4.1 Description of the Specified Dynamics – Whole Atmosphere Community** 14 **Climate Model**

15 The latest version of the NCAR Community Earth System Model, version 1 (CESM1)
16 Specified Dynamics – Whole Atmosphere Community Climate Model (SD-WACCM) was
17 used to predict the impact of GCRs on the atmosphere. SD-WACCM is a global model with
18 88 vertical levels from the surface to 4.5x10⁻⁶ hPa (approximately 140 km geometric height).
19 SD-WACCM was most recently described in Wegner et al. (2013) and Solomon et al. (2015)
20 and uses prescribed dynamical fields (e.g., see Lamarque et al., 2012) from the NASA Global
21 Modeling and Assimilation Office Modern-Era Retrospective Analysis for Research and
22 Applications (MERRA) (Rienecker et al., 2011). Temperature, zonal and meridional winds,
23 and surface pressure are used to drive the physical parameterizations that control boundary
24 layer exchanges, advective and convective transport, and the hydrological cycle. The SD-
25 WACCM meteorological fields are relaxed toward the MERRA reanalysis fields using the
26 approach described in Kunz et al. (2011).

27 The chemical module of SD-WACCM is based upon the 3-D chemical transport Model of
28 Ozone and Related Tracers, Version 3 (MOZART) (Kinnison et al., 2007). It includes a
29 detailed representation of the chemical and physical processes from the troposphere through
30 the lower thermosphere. The species included within this mechanism are contained within the
31 O_x, NO_x, HO_x, ClO_x, and BrO_x chemical families, along with CH₄ and its degradation

1 products. SD-WACCM also includes 17 primary nonmethane hydrocarbons and related
2 oxygenated organic compounds (Emmons et al., 2010). This mechanism contains 134 species,
3 420 chemical reactions, with 17 heterogeneous reactions on multiple aerosol types (i.e.,
4 sulfate, nitric acid trihydrate, and water-ice; Solomon et al., 2015). Reaction rates have been
5 updated to JPL-2010 (Sander et al., 2011). Tropospheric NO_x production from lightning and
6 aircraft is included as described in Lamarque et al. (2012).

7 For this work, the SPARC Chemistry Climate Model Initiative (CCMI), REFC1 scenario was
8 used (see Eyring et al., 2013). This scenario included observed time-dependent evolution of:
9 greenhouse gases (GHGs); ozone depleting substances (ODSs); sea surface temperatures and
10 sea ice concentrations (SSTs/SICs); stratospheric sulfate surface area densities (SADs); and
11 11-year solar cycle variability, which includes spectrally resolved solar irradiances.

12 **4.2 Description of the Goddard Space Flight Center Two-Dimensional Model**

13 The most recent version of the Goddard Space Flight Center (GSFC) two-dimensional (2-D)
14 atmospheric model was used to predict the impact of GCRs on the atmosphere. This model
15 was first discussed over 25 years ago (Douglass et al. 1989; Jackman et al. 1990) and has
16 undergone extensive improvements over the years (e.g., Considine et al. 1994; Jackman et al.
17 1996; Fleming et al. 1999, 2007, 2011, 2015). The vertical range of the model, equally
18 spaced in log pressure, is from the ground to approximately 92 km (0.0024 hPa) with about a
19 1 km grid spacing. The model has a 4° latitude grid spacing.

20 The specified transport version of the model is used for this study. Here, the model transport
21 fields are derived using daily average global winds and temperatures from the National
22 Centers for Environmental Prediction-National Center for Atmospheric Research (NCEP-
23 NCAR) reanalysis project for years 1960-1978 (Kalnay et al. , 1996; Kistler et al. , 2001)) and
24 the MERRA meteorological analyses for years 1979-2010. Thirty-day running averages of
25 the residual circulation, eddy diffusion, zonal mean wind, and zonal mean temperature are
26 computed using the methodology detailed in Fleming et al. (2007). For use in some of the
27 simulations a climatological average was constructed of the transport over these years and
28 applied it over the simulated periods. The averaged transport fields change daily, but repeat
29 yearly.

30 The ground boundary conditions in the GSFC 2-D model for the ozone depleting substances
31 are taken from WMO (2014) for years 1960-2010. The model uses a chemical solver

1 described in Jackman et al. (2005) and Fleming et al. (2007, 2011). For these computations,
2 the photochemical gas and heterogeneous reaction rates and photolysis cross sections have
3 been updated to the Jet Propulsion Laboratory recommendations (Sander et al., 2011) with
4 further updates based on SPARC (2013).

5 The model tropospheric chemistry scheme has also been updated to include the following
6 species: CH₃OH, C₂H₆, CH₃CHO, CH₃CO₃, CH₃C(O)OOH, CH₃CO₃NO₂ (peroxy acetyl
7 nitrate, PAN), C₂H₅O₂, C₂H₅OOH, CH₃COCH₃ (acetone), and C₅H₈ (isoprene). For this, the
8 following quantities are specified using a four-year average (2004-2007) of output from
9 recent simulations of the Global Modeling Initiative's (GMI) combined stratosphere-
10 troposphere chemistry and transport model (Strahan et al., 2007; Duncan et al., 2007; Strode
11 et al. 2015): surface emissions of CH₂O, CO, NO_x, C₂H₆, and isoprene; surface mixing ratio
12 boundary conditions for acetone, and tropospheric NO_x production from lightning and
13 aircraft. The model tropospheric OH is specified from the monthly varying OH field
14 documented in Spivakovsky et al. (2000). Surface dry deposition rates for H₂O₂, CH₂O,
15 CH₃OOH, HNO₃, NO₂, N₂O₅, PAN, and O₃, and tropospheric washout rates for HO₂, H₂O₂,
16 CH₂O, CH₃OOH, HONO, HNO₃, HO₂NO₂, NO₂, NO₃, and N₂O₅ are also specified from the
17 GMI output. The resulting 2-D distributions of tropospheric NO_x and ozone (as well as HNO₃,
18 CO, C₂H₆, and PAN) compare well with the GMI simulations and the ozone climatology
19 compiled by McPeters et al. (2007). This allows the model to be used to simulate the GCR
20 perturbations in the stratosphere and troposphere addressed in this study.

21 **4.3 Model simulations**

22 We conducted fourteen model simulations with the two models, which are all briefly
23 described in Table 1. SD-WACCM was used for two simulations, both over the period 2000-
24 2010. One of the SD-WACCM simulations did not include GCRs (simulation *Base_SD-W*),
25 whereas the other did (simulation *GCR_SD-W*).

26 The GSFC 2-D model was used for twelve simulations, all over the 51-year period 1960-
27 2010. The transport was specified for all simulations, either interannually varying with
28 NCEP-NCAR data for years 1960-1978 and with MERRA data for years 1979-2010 or with a
29 climatological average of those data over the 1960-2010 time period. Five of the simulations
30 (labeled **_Base_GSFC*) did not include GCRs and seven of the simulations (labeled
31 **_GCR_GSFC*) did include GCRs. Four simulations (*AI_GCR_GSFC*, *BI_GCR_GSFC*,

1 *C_GCR_GSFC*, and *D_GCR_GSFC*) used a 51-year average of the GCR amount and three
2 simulations (*A2_GCR_GSFC*, *B2_GCR_GSFC*, and *E_GCR_GSFC*) included the interannual
3 variation of GCRs. These simulations investigated the impact of GCRs in a changing
4 atmosphere of different chlorine-loading, sulfate aerosol amount, solar photon flux, and
5 dynamics over this time period.

6 **5 Results**

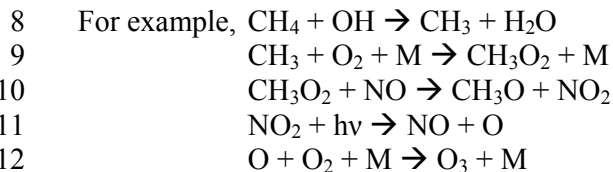
7 SD-WACCM and GSFC 2-D model simulations were compared to delineate the GCR-caused
8 changes under different atmospheric conditions. Model simulations were compared for the
9 year 2009 (solar minimum, GCR maximum) to determine the GCR impact on several
10 constituents in section 5.1. The influence of GCRs over the solar cycle is also shown in
11 section 5.1 (comparing year 2009 to year 2002). Changing atmospheric conditions over the
12 years 1960-2010 and their impact on the GCR atmospheric influence are shown in section 5.2.
13 In particular, GCR-caused global total ozone changes in the different regions of the
14 atmosphere (troposphere, stratosphere, and total) are discussed in section 5.2 as well as the
15 global total ozone changes caused by GCRs with different imposed atmospheric conditions.
16 Finally, the GCR-caused NO_y production is given in comparison to the N₂O oxidation-caused
17 NO_y production in section 5.3.

18 **5.1 NO_x, Ozone, HO_x, and HNO₃**

19 The GCR-caused NO_x (NO+NO₂) impact is shown in Figure 4 (top) for SD-WACCM and in
20 Figure 5 (top) for the GSFC 2-D model. NO_x is mostly enhanced throughout the domain from
21 1000-1 hPa with largest increases (>15%) in the south polar troposphere. GCR-caused NO_x
22 increases over 6% are computed in the north polar lower stratosphere. Although there are
23 differences between the SD-WACCM and GSFC 2-D model computations shown here and
24 those computed by Calisto et al. (2011), there are many similarities including the larger
25 computed GCR-caused NO_x impact in the south polar tropospheric region compared with the
26 north polar tropospheric region. The larger percentage change in the SH polar (60-90°S)
27 troposphere is due to this region being significantly cleaner (NO_x background levels of 5-20
28 pptv) compared to north polar (60-90°N) troposphere (background levels of 20-50 pptv). As
29 an aside, the SD-WACCM results, like those in Calisto et al. (2011), indicate a much smaller
30 GCR-caused NO_x impact than computed in Semeniuk et al. (2011). Mironova et al. (2015)
31 propose that “the absence of anthropogenic and natural NO_x emissions together with

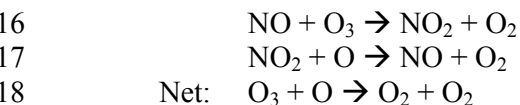
1 oversimplified tropospheric chemistry in CMAM” may be the reason for the larger response
2 of the GCR perturbation in CMAM.

3 The GCR-caused ozone impact is shown in Figure 4 (bottom) for SD-WACCM and in Figure
4 5 (bottom) for the GSFC 2-D model. Ozone is mostly enhanced in the troposphere and lowest
5 part of the stratosphere with largest increases of 1-2% from GCRs in the south polar
6 troposphere in 2009. The GCR-caused ozone increase is due to two processes: 1) the NO
7 reacting with CH₄ oxidation products (see, also Krivolutsky et al., 2001):



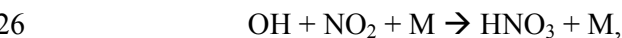
13 and 2) the GCR-produced NO₂ reacts with ClO to form ClONO₂ and reduces the chlorine-
14 caused ozone loss.

15 Ozone is decreased in most of the stratosphere due to the NO_x catalytic ozone depletion cycle:



19 GCR-caused NO_x increases of ~1-6% are calculated for the lower stratosphere and cause
20 ozone decreases of 0.2-1%. Our computed ozone impacts are similar to those previously
21 discussed in Krivolutsky et al. (2001) and Calisto et al. (2011).

22 The computed impact of GCRs on HO_x and HNO₃ using SD-WACCM is given in Figure 6.
23 Although GCRs produce HO_x (see section 3), HO_x decreases are computed throughout most
24 of the atmosphere (Figure 6, top). This is caused by the NO_x increases which remove OH via
25 the reaction



27 leading to HNO₃ enhancements (Figure 6, bottom). Again, these results are similar to those
28 discussed in Calisto et al. (2011).

29 The SD-WACCM computations can also be used to address the question of the change in
30 GCR influence over a solar cycle. The focus in this section has been on year 2009 since that
31 was near solar minimum resulting in the maximum atmospheric influences caused by GCRs.
32 The last previous solar maximum or GCR minimum occurred in year 2002. Since the
33 background atmosphere changes significantly from year 2002 to year 2009, it would be

1 confusing to directly compare atmospheric changes between the two years to derive any
2 GCR-caused change. Instead, the annual average percentage change from GCRs was
3 computed for years 2002 and 2009 separately and then differenced from each other to
4 illustrate the GCR-caused change over the solar cycle. The results are given in Figure 7 for
5 NO_x (top) and ozone (bottom) using simulations *GCR_SD-W* and *BASE_SD-W*. The
6 computed GCR-induced solar cycle changes from 2002 to 2009 were slightly smaller than
7 those computed for the GCR-maximum (solar minimum) year 2009. The GCR-caused
8 changes are proportional to the GCR-caused ion pair production, which is given in Figure 1
9 for the years 2002 and 2009. Note that the largest ion pair production near the south pole is
10 over $30 \text{ cm}^{-3}\text{s}^{-1}$ in 2009 and is nearly $15 \text{ cm}^{-3}\text{s}^{-1}$ in 2002. Thus, there is a difference of about
11 $15 \text{ cm}^{-3}\text{s}^{-1}$ from 2002 to 2009 versus a difference of $30 \text{ cm}^{-3}\text{s}^{-1}$ for 2009 in a comparison
12 without GCRs to with GCRs.

13 **5.2 Time-dependent Total Ozone Changes**

14 The GSFC 2-D model gives fairly similar results to SD-WACCM (compare Figs. 4 and 5) and
15 is significantly faster computationally to use for longer-term simulations. Thus, the GSFC 2-D
16 model was used in several sensitivity study simulations described in Table 1 (and Sect. 4.2) to
17 investigate the longer term GCR-caused changes, particularly focusing on annual average
18 global total ozone (AAGTO) as well as global column ozone in the two regions between 1000
19 and 100 hPa and between 100 and 1 hPa. The GCR-caused change in ozone in those two
20 regions, separately, and for the entire troposphere and stratosphere (1000 to 1 hPa) is
21 computed for two pairs of scenarios: (1) Fig. 8 (top) shows a comparison of the first pair
22 (A1_GCR_GSFC to A_Base_GSFC), which are simplified representations of the atmosphere
23 with a climatological mean transport (changes daily, but repeats yearly) in both scenarios and
24 a mean GCR input (constant throughout the simulation) in A1_GCR_GSFC; and (2) Fig. 8
25 (bottom) shows a comparison of the most comprehensive pair (E_GCR_GSFC to
26 E_Base_GSFC), which include interannually varying transport, sulfate aerosol surface area,
27 and solar cycle photon flux variation in both scenarios and an interannually varying GCR
28 input in E_GCR_GSFC.

29 First, focus on the results intercomparing scenarios A1_GCR_GSFC to A_Base_GSFC (see
30 Fig. 8, top): the GCR-caused column ozone between 1000 and 100 hPa showed an increase
31 from +0.03% up to \sim +0.05% over the 1960–2010 time period, driven partly by increases in
32 CH_4 over those 51 years. The GCR-caused column ozone between 100 and 1 hPa also

1 showed a time dependent increase, but started in year 1960 at -0.19% ending up at -0.12% in
2 year 2010. The GCR-caused total AAGTO follows the increases in the two regions noted
3 above, starting at -0.16% in year 1960 and increasing to \sim -0.07% in year 2010.

4 Second, intercompare the more complete simulations E_GCR_GSFC to E_Base_GSFC (see
5 Fig. 8, bottom): the GCR-caused column ozone changes between 1000 and 100 hPa showed a
6 significant variation from \sim +0.03% to \sim +0.07% over the 1960–2010 time period. The GCR-
7 caused column ozone changes between 100 and 1 hPa also showed substantial variation
8 giving -0.23% in 1979 and -0.02% in 1992. The GCR-caused total AAGTO followed these
9 variations, with a low of -0.19% in 1979 and a high of +0.03% in 1992.

10 The GCR-caused atmospheric changes are larger at higher latitudes, thus we also compute the
11 annual average polar total ozone (AAPTO). The AAPTO is calculated using the model
12 output only at polar latitudes (60-90 degrees South and 60-90 degrees North) and is given in
13 Figure 9. Both the AAGTO (Figure 8) and the AAPTO (Figure 9) have similar shapes for the
14 total ozone change in the two regions plotted (1000 to 100 hPa and 100 to 1 hPa). In 1960 the
15 AAGTO for the entire troposphere and stratosphere (1000 to 1 hPa) is computed to be -0.13%
16 (see Figure 8, bottom) while the AAPTO is computed to be -0.18% (see Figure 9, bottom). In
17 2010 the AAGTO for the troposphere and stratosphere is computed to be -0.11% (see Figure
18 8, bottom) while the AAPTO is computed to be -0.27% (see Figure 9, bottom). Thus, the
19 polar differences tend to be larger by the end than they were at the start of the simulation
20 period.

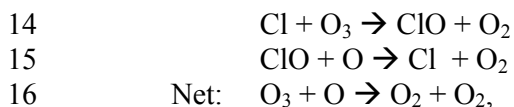
21 The impact of five simultaneous atmospheric changes are responsible for the GCR-caused
22 variations in AAGTO observed in Figure 8(bottom). These changes are: 1) background total
23 chlorine; 2) sulfate aerosol surface area; 3) solar cycle photon flux variation; 4) solar cycle
24 GCR variation; and 5) interannual transport variability. Background total chlorine increases
25 dramatically from 0.7 to 3.5 ppbv over the 1960-2010 period (Figure 10A, Equator, 1 hPa).
26 Volcanoes can add substantially to the aerosol surface area during certain years (especially
27 1963, 1982, and 1991, see Figure 10B). The photon flux varies over the solar cycle and is
28 especially important to the stratosphere at ultraviolet wavelengths. The solar flux variation at
29 200 nm (up to about 8.5% from solar minimum to maximum) is important for ozone
30 production and is shown in Figure 10C. The GCRs vary over the solar cycle as well and the
31 GCR-caused ion pair production is given in Figure 10D at 200 hPa and 90°S. The final

1 atmospheric variation is due to the interannual transport variability over the whole time
2 period, which is difficult to illustrate in a line plot (like those given in Figure 10).

3 **5.2.1 Background total chlorine**

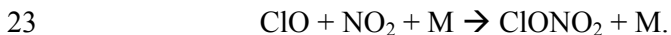
4 The smoothest change over the 1960-2010 time period occurred with the amount of
5 background total chlorine. The AAGTO has been computed for the six scenarios
6 (*A_Base_GSFC*, *A1_GCR_GSFC*, *A2_GCR_GSFC*, *B_Base_GSFC*, *B1_GCR_GSFC*,
7 *B2_GCR_GSFC*) for use in this analysis. Percentage differences in AAGTO for
8 *A1_GCR_GSFC* compared to *A_Base_GSFC* are shown in Figure 11A (black solid line)
9 compared with background total chlorine (red solid line). Note the good correspondence
10 between background total chlorine amount and GCR-caused AAGTO change. Smaller
11 amounts of background total chlorine correlate with larger computed GCR-caused AAGTO
12 decrease and vice versa.

13 First, this is partly a reflection of the role that chlorine, through the ClO_x catalytic cycle



17 has in controlling stratospheric ozone over this time period. At low levels of chlorine, the
18 NO_x catalytic cycle is more important to ozone control. Thus, increases in NO_x, such as
19 caused by GCRs, lead to a more significant ozone response in the 1960s than in the 2000s
20 when the background total chlorine amounts are much higher.

21 Second, this is also a reflection of the interference of the NO_x family with the ClO_x catalytic
22 cycle through the reaction



24 Increased NO_x amounts caused by GCRs will lead to an increased production of the reservoir
25 constituent, ClONO₂, and thus less ozone destruction.

26 Both of these processes are ongoing in the atmosphere and are reflected in Figure 11A, which
27 illustrates most clearly the correlation between the GCR-caused change in ozone and
28 background total chlorine amount.

29 Figure 11B shows the results of the AAGTO computed in *B1_GCR_GSFC* compared to
30 *B_Base_GSFC*. The main difference here is that the model transport changes interannually.

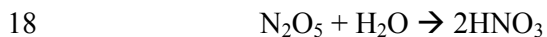
1 There still is a correlation between high background total chlorine amounts and less AAGTO
2 change caused by the GCRs.

3 Figure 11C illustrates the results of a comparison of the AAGTO computed in
4 *A2_GCR_GSFC* compared to *A_Base_GSFC*. Both simulations have the same mean
5 transport imposed over the 51-year time period, however, the GCRs are forced with
6 interannually varying GCRs (see Figure 10D). Again, there is a correspondence between the
7 amount of background total chlorine and the GCR-caused AAGTO change.

8 Finally, Figure 11D illustrates the results of a comparison of the AAGTO computed in
9 *B2_GCR_GSFC* compared to *B_Base_GSFC*. Both simulations have interannual transport
10 and the simulation with GCRs (*B2_GCR_GSFC*) includes the interannual variation of GCRs.
11 Although there is clearly more year-to-year variability, it is apparent that higher background
12 total chlorine levels lead to less GCR-caused ozone changes.

13 **5.2.2 Aerosol surface area**

14 The aerosol surface area varies dramatically over the 1960-2010 time period. Volcanoes in
15 years 1963, 1982, and 1991 caused large increases in the aerosol surface area. Enhanced
16 aerosol surface area results in an increase in heterogeneous reactions on the sulfate aerosols.
17 In particular, the reaction



19 proceeds rapidly, taking the more active NO_x constituents and producing the less active HNO₃
20 reservoir constituent. The result of this is that NO_x production from any source is less
21 efficient. A comparison of the AAGTO computed in *C_GCR_GSFC* compared to
22 *C_Base_GSFC* is shown in Figure 12. This shows that the GCRs cause a less negative
23 change (even positive in 1992-3) in AAGTO during the years of enhanced aerosol surface
24 area.

25 **5.2.3 Solar cycle photon variation**

26 The sun not only influences the GCR flux over a solar cycle, but it also shows a significant
27 variation in solar photons and solar particles (electrons, protons and other particles). The
28 photon flux variation and its impact on the GCR effect will be addressed here. However, it is
29 outside the scope of this paper to discuss the influence of solar energetic particles (e.g.,
30 protons, other ions, and electrons) on the GCR-caused atmospheric influence.

1 The solar cycle variation led to changes in the photon flux, especially at the X-ray, extreme
2 ultraviolet, and ultraviolet wavelengths. In particular, the stratosphere is greatly influenced
3 by photons at ultraviolet wavelengths (e.g., 200 nm photons are important in producing
4 ozone) and a variation of up to about 8.5% from solar minimum to maximum was shown in
5 Figure 10C. A comparison of the AAGTO computed in *D_GCR_GSFC* was compared to
6 *D_Base_GSFC*. These simulations isolated the impact of the solar cycle photon variation on
7 the GCR influence. Only a very minor change ($\pm 0.004\%$ in AAGTO) was found to be
8 forced by the solar cycle photon flux variation (not shown).

9 **5.2.4 GCR interannual and solar cycle driven variation**

10 The GCRs vary from year-to-year, influenced primarily by the strength of the solar magnetic
11 field. The GCR variation (given in ion pair production) can be as large as a factor of two at
12 the poles (see Figure 10D). Most of the impact from GCRs is in the polar lower stratosphere/
13 upper troposphere, since the GCR caused ionization rates peak there (see Figure 1). The
14 residence time for constituents in the lower stratosphere is long (~ 1 year or so, which is driven
15 by the transport) as is the photochemical time constant for odd oxygen (essentially ozone) in
16 this region (e.g., see Figure 5.3, Brasseur and Solomon, 1995), thus the computed impact of
17 the GCRs on the atmosphere will be a time-lagged average of the GCR input. The AAGTO
18 shown in Figure 11C was differenced from that shown in Figure 11A in order to compute the
19 change caused by the interannual GCR variation. This interannually-driven GCR change in
20 AAGTO is represented by the black line in Figure 13. The red line in Figure 13 is a two-year
21 boxcar (running) average of the GCR ion pair production (in $\text{cm}^{-3}\text{s}^{-1}$) at 200 hPa and 90°S
22 with a one-year lag and appears to be an anti-correlation of the AAGTO change. Thus, the
23 impact of the interannual variation in the GCRs with an imposed one-year time lag and two-
24 year average can represent the computed AAGTO change fairly well.

25 **5.2.5 Interannual transport variation**

26 The interannual transport variation drives changes in the impact of the GCRs on the AAGTO.
27 This interannual behavior is best observed in Figure 11B, where the mean GCRs are imposed
28 continuously over the entire 51-year time period. Variations of up to $\sim 0.04\%$ in the GCR-
29 caused AAGTO impact are computed over a couple of years or so. However as noted in
30 section 5.3.1, the strong correlation between high background total chlorine amounts and less
31 AAGTO change caused by the GCRs dominates so that the interannual transport changes
32 have only a very small effect on the time-dependent GCR-induced AAGTO impact.

1 **5.3 NO_y Production**

2 The total NO_y produced per year from GCRs was compared with that from other sources.
3 GSFC 2-D model calculations show that N₂O oxidation ($\text{N}_2\text{O} + \text{O}(^1\text{D}) \rightarrow \text{NO} + \text{NO}$) produce
4 43.5-55.7 GigaMoles of NO_y with the vast majority (greater than 90%) produced in the
5 stratosphere. GCRs were computed to produce 3.1-6.4 GigaMoles of NO_y, with 40-50% of
6 that produced in the stratosphere. Thus, GCRs can be responsible for as much as 14% of the
7 total NO_y production, however on average, GCRs produce about 3-6% of stratospheric NO_y in
8 any given year. This is somewhat less than that found by Vitt and Jackman (1996), who
9 computed that GCRs were responsible for 9-12% of the total stratospheric NO_y produced per
10 year. The Vitt and Jackman (1996) computations used ion pair production rates from a
11 parameterization based on yearly averaged sunspot number from Nicolet (1975), which are
12 generally larger than those GCR-caused ion pair production rates computed with the more
13 recent NAIRAS model (discussed in section 2).

14 **6 Conclusions**

15 Two global models, SD-WACCM and GSFC 2-D, were used to study the atmospheric impact
16 of GCRs over the 1960-2010 time period. The largest atmospheric impacts occurred in the
17 NO_x constituents, which had maximum GCR-caused increases of 4-15% in the Southern
18 polar troposphere. There were associated ozone increases of 1-2% correlated with these NO_x
19 enhancements. The lower stratosphere was also impacted with computed NO_x increases of
20 ~1-6% causing associated ozone decreases of 0.2-1%. GCR-caused decreases of AAGTO
21 were computed to be 0.2% or less with GCR-caused tropospheric column ozone increases of
22 0.08% or less and GCR-caused stratospheric column ozone decreases of 0.23% or less. There
23 appears to be a time lag of about a year between the GCR-caused NO_x production and the
24 resultant AAGTO change. This is consistent with the long residence and photochemical time
25 constant of ozone in the lower stratosphere. The impact of GCRs has a strong correlation with
26 the atmospheric chlorine loading, sulfate aerosol loading, and solar cycle variation. GCRs
27 cause larger atmospheric impacts with less chlorine loading, less sulfate aerosol loading, and
28 for years closer to solar minimum.

29 **Acknowledgements**

30 CHJ, DRM, DEK, CJM, and ELF thank the NASA Headquarters Living With a Star Targeted
31 Research and Technology Program for support during the time that this manuscript was
32 written. CHJ and ELF were also supported by the NASA Headquarters Atmospheric

1 Composition Modeling and Analysis Program. The National Center for Atmospheric
2 Research (NCAR) is sponsored by the U.S. National Science Foundation. WACCM is a
3 component of the Community Earth System Model (CESM), which is supported by the
4 National Science Foundation (NSF) and the Office of Science of the U.S. Department of
5 Energy. Computing resources were provided by NCAR's Climate Simulation Laboratory,
6 sponsored by NSF and other agencies. This research was enabled by the computational and
7 storage resources of NCAR's Computational and Information System Laboratory (CISL).
8

1 References

- 2 Badhwar, G. D. and O'Neill, P. M.: An improved model of galactic cosmic radiation for
3 space exploration missions, *Nuclear Tracks Radiat. Mea*, **20**, 403-410, 1992.
- 4 Badhwar, G. D. and O'Neill, P. M.: Long term modulation of galactic cosmic radiation and its
5 model for space exploration, *Adv. Space Res.*, **14**, 749-757, 1994.
- 6 Badhwar, G. D. and O'Neill, P. M.: Galactic cosmic radiation model and its applications, *Adv.*
7 *Space Res.*, **17**, 7-17, 1996.
- 8 Brasseur, G., and Solomon, S.: Aeronomy of the Middle Atmosphere: Chemistry and Physics
9 of the Stratosphere and Mesosphere, D. Reidel Publishing Company, Dordrecht, The
10 Netherlands, 1995.
- 11 Calisto, M., Usoskin, I., Rozanov, E., and Peter, T.: Influence of Galactic Cosmic Rays on
12 atmospheric composition and dynamics, *Atmos. Chem. Phys.*, **11**, 4547-4556, 2011.
- 13 Considine, D. B., Douglass, A. R., and Jackman, C. H.: Effects of a polar stratospheric cloud
14 parameterization on ozone depletion due to stratospheric aircraft in a two-dimensional
15 model, *J. Geophys. Res.*, **99**, 18,879– 18,894, 1994.
- 16 Douglass, A. R., Jackman, C. H., and Stolarski, R. S.: Comparison of model results
17 transporting the odd nitrogen family with results transporting separate odd nitrogen
18 species, *J. Geophys. Res.*, **94**, 9862-9872, 1989.
- 19 Duncan, B.N., Strahan, S.E., Yoshida, Y., Steenrod, S.D., and Livesey, N.: Model study of
20 the cross-tropopause transport of biomass burning pollution, *Atmos. Chem. Phys.*, **7**,
21 3713–3736, doi:10.5194/acp-7-3713-2007, 2007.
- 22 Emmons, L. K., Walters, S., Hess, P. G., Lamarque, J.-F., Pfister, G. G., Fillmore, D.,
23 Granier, C., Guenther, A., Kinnison, D., Laepple, T., Orlando, J., Tie, X., Tyndall, G.,
24 Wiedinmyer, C., Baughcum, S. L., and Kloster, S.: Description and evaluation of the
25 Model for Ozone and Related chemical Tracers, version 4 (MOZART-4), *Geosci.*
26 *Model Dev.*, **3**, 43–67, doi:10.5194/gmd-3-43-2010, 2010.
- 27 Eyring, V., Lamarque, J.-F., Hess, P., Arfeuille, F., Bowman, K., Chipperfield, M., Duncan,
28 B., Fiore, A., Gettelman, A., Giorgetta, M., Granier, C., Hegglin, M., Kinnison, D.,
29 Kunze, M., Langematz, U., Luo, B., Martin, R., Matthes, K., Newman, P., Peter, T.,
30 Robock, A., Ryerson, T., Saiz-Lopez, A., Salawitch, R., Schultz, M., Shepherd, T. G.,
31 Shindell, D., Staehelin, J., Tegtmeier, S., Thomason, L., Tilmes, S., Vernier, J.-P.,
32 Waugh, D. W., and Young, P. J.: Overview of IGAC/SPARC Chemistry-Climate
33 Model Initiative (CCMI) Community Simulations in Support of Upcoming Ozone and
34 Climate Assessments, SPARC newsletter, n40, pg48-66, Zurich, Switzerland, January
35 2013.
- 36 Finlay, C. C., Maus, S., Beggan, C. D., Bondar, T. N., Chambodut, A., Chernova, T.
37 A., Chulliat, A., Golovkov, V. P., Hamilton, B., Hamoudi, M., Holme, R., Hulot, G.,
38 Kuang, W., Langlais, B., Lesur, V., Lowes, F. J., Lühr, H., Macmillan, S., Mandea,
39 M., McLean, S., Manoj, C., Menvielle, M., Michaelis, I., Olsen, N., Rauberg, J.,
40 Rother, M., Sabaka, T. J., Tangborn, A., Tøffner-Clausen, L., Thébaud, E., Thomson, A.
41 W. P., Wardinski, I., Wei, Z., and Zvereva, T. I.: International Geomagnetic Reference
42 Field: the eleventh generation, *Geophysical Journal International*, **183**, 1216-1230,
43 doi:10.1111/j.1365-246X.2010.04804, 2010.
- 44 Fleming, E. L., Jackman, C. H., Considine, D. B., and Stolarski, R. S.: Simulation of
45 stratospheric tracers using an improved empirically based two-dimensional model
46 transport formulation, *J. Geophys. Res.*, **104**, 23911-23934, 1999.

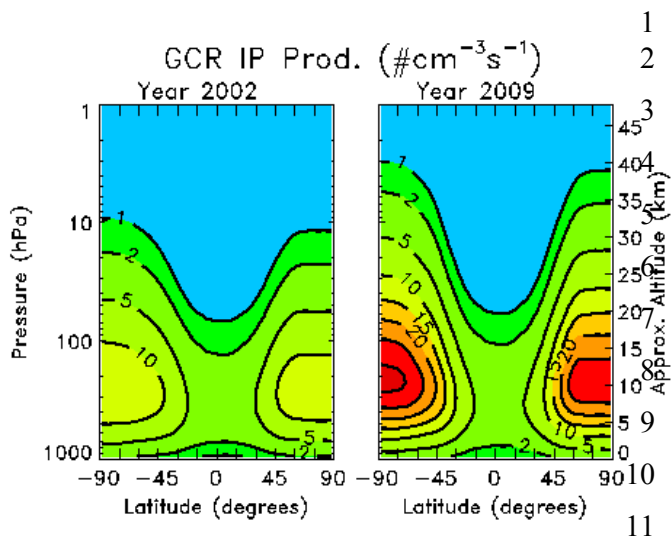
- 1 Fleming, E. L., Jackman, C. H., Weisenstein, D. K., and Ko, M. K. W.: The impact of inter-
2 annual variability on multidecadal total ozone simulations, *J. Geophys. Res.*, *112*,
3 D10310, doi:10.1029/2006JD007953, 2007.
- 4 Fleming, E. L., Jackman, C. H., Stolarski, R. S., and Douglass, A. R.: A model study of the
5 impact of source gas changes on the stratosphere for 1850-2100, *Atmos. Chem. Phys.*
6 *11*, 8515-8541, 2011.
- 7 Fleming, E. L., George, C., Heard, D. E., Jackman, C. H., Kurylo, M. J., Mellouki, W., Orkin,
8 V. L., Swartz, W. H., Wallington, T. J., Wine, P. H., and Burkholder, J. B.: The impact
9 of current CH₄ and N₂O atmospheric loss process uncertainties on calculated ozone
10 abundances and trends, *J. Geophys. Res. Atmos.*, *120*, 5267–5293,
11 doi:10.1002/2014JD022067, 2015.
- 12 Garcia, R. R., Solomon, S., Roble, R. G., and Rusch, D. W.: A numerical response of the
13 middle atmosphere to the 11-year solar cycle, *Planet. Space Sci.*, *32*, 411-423, 1984.
- 14 Jackman, C. H.: Effects of energetic particles on minor constituents of the middle atmosphere,
15 *J. Geomag. Geoelectr.*, *43*, Suppl., 637-646, 1991.
- 16 Jackman, C. H.: Energetic particle influences on NO_y and Ozone in the middle atmosphere,
17 *Interactions Between Global Climate Subsystems, The Legacy of Hann, Geophysical*
18 *Monograph 75, IUGG Volume 15*, 131-139, 1993.
- 19 Jackman, C. H., Frederick, J. E., and Stolarski, R. S.: Production of odd nitrogen in the
20 stratosphere and mesosphere: An intercomparison of source strengths, *J. Geophys.*
21 *Res.*, *85*, 7495-7505, 1980.
- 22 Jackman, C. H., Guthrie, P. D., and Kaye, J. A.: An intercomparison of nitrogen-containing
23 species in Nimbus 7 LIMS and SAMS data, *J. Geophys. Res.*, *92*, 995-1008, 1987.
- 24 Jackman, C. H., Douglass, A. R., Rood, R. B., McPeters, R. D., and Meade, P. E.: Effect of
25 Solar Proton Events on the Middle Atmosphere During the Past Two Solar Cycles as
26 Computed Using a Two-dimensional Model, *J. Geophys. Res.*, *95*, 7417-7428, 1990.
- 27 Jackman, C. H., Fleming, E. L., Chandra, S., Considine, D. B., and Rosenfield, J. E.: Past,
28 present, and future modeled ozone trends with comparisons to observed trends, *J.*
29 *Geophys. Res.*, *101*, 28753-28767, 1996.
- 30 Jackman, C. H., DeLand, M. T., Labow, G. J., Fleming, E. L., Weisenstein, D. K., Ko, M. K.
31 W., Sinnhuber, M., and Russell, J. M.: Neutral atmospheric influences of the solar
32 proton events in October-November 2003, *J. Geophys. Res.*, *110*, A09S27,
33 doi:10.1029/2004JA010888, 2005.
- 34 Kalnay, E., Kanamitsu, M., Kistler, R., Collins, W., Deaven, D., Gandin, L., Iredell, M., Saha,
35 S., White, G., Woollen, J., Zhu, Y., Chelliah, M., Ebizusaki, W., Higgins, W.,
36 Janowiak, J., Mo, K. C., Ropelewski, C., Wang, J., Leetmaa, A., Reynolds, R., Jenne,
37 R., and Joseph, D.: The NCEP/NCAR 40-year reanalysis project, *Bull. Am. Meteor.*
38 *Soc.*, *77*, 437-471, 1996.
- 39 Kistler, R., Collins, W., Saha, S., White, G., Woollen, J., Kalnay, E., Chelliah, M., Ebizusaki,
40 W., Kanamitsu, M., Kousky, V., van den Dool, H., Jenne, R., and Fiorino, M.: The
41 NCEP-NCAR 50-year reanalysis: Monthly means CD-ROM and documentation, *Bull.*
42 *Am. Meteor. Soc.*, *82*, 247-267, 2001.
- 43 Kinnison, D. E., Brasseur, G. P., Walters, S., Garcia, R. R., Marsh, D. R., Sassi, F., Harvey,
44 V. L., Randall, C. E., Emmons, L., Lamarque, J. F., Hess, P., Orlando, J. J., Tie, X. X.,
45 Randel, W., Pan, L. L., Gettelman, A., Granier, C., Diehl, T., Niemeier, U., and
46 Simmons, A. J.: Sensitivity of chemical tracers to meteorological parameters in
47 the MOZART-3 chemical transport model, *J. Geophys. Res.*, *112*, D20302,
48 doi:10.1029/2006JD007879, 2007.

- 1 Krivolutsky, A. A., Kuminov, A. A., and Repnev, A. I.: Effects of Cosmic Rays on the
2 Earth's Ozonosphere: A Review, *Geomagnetism and Aeronomy*, **39**, 271-282, 1999.
- 3 Krivolutsky, A. A., Bazilevskaya, G. A., Vyushkova, T. Y., and Knyazeva, G. V.: Long-term
4 tropospheric variations of ozone content caused by galactic cosmic ray influence, *Adv.*
5 *Space Res.*, **27**, 2019-2024, 2001.
- 6 Krivolutsky, A., Bazilevskaya, G., Vyushkova, T., and Knyazeva, G.: Influence of cosmic
7 rays on chemical composition of the atmosphere: data analysis and photochemical
8 modeling, *Phys. Chem. Earth*, **27**, 471-476, 2002.
- 9 Kunz, A., Pan, L., Konopka, P., Kinnison, D. E., and Tilmes, S.: Chemical and dynamical
10 discontinuity at the extratropical tropopause based on START08 and WACCM
11 analysis, *J. Geophys. Res.*, **116**, D24302, doi:10.1029/2011JD016686, 2011.
- 12 Lamarque, J.-F., Emmons, L. K., Hess, P. G., Kinnison, D. E., Tilmes, S., Vitt, F., Heald, C.
13 L., Holland, E. A., Lauritzen, P. H., Neu, J., Orlando, J. J., Rasch, P. J., and Tyndall,
14 G. K.: CAM-chem: Description and evaluation of interactive atmospheric chemistry in
15 the Community Earth System Model, *Geosci. Model Dev.*, **5**, 369-411,
16 doi:10.5194/gmd-5-369-2012, 2012.
- 17 Legrand, M. R., Stordal, F., Isaksen, I. S. A., and Rognerud, B.: A model study of the
18 stratospheric budget of odd nitrogen, including effects of solar cycle variations, *Tellus*,
19 **41B**, 413-426, 1989.
- 20 McPeters, R.D., Labow, G.J., and Logan, J.A.: Ozone climatological profiles for satellite
21 retrieval algorithms, *J. Geophys. Res.*, **112**, D05308, doi:10.1029/2005JD006823,
22 2007.
- 23 Mertens, C. J., Kress, B. T., Wiltberger, M., Tobiska, W. K., Grajewski, B., and Xu, X.:
24 Atmospheric ionizing radiation from galactic and solar cosmic rays, Current Topics in
25 Ionizing Radiation Research, Edited by Mitsuru Neno, InTech Publisher (ISBN 978-
26 953-51-0196-3), 2012.
- 27 Mertens, C. J., Meier, M. M., Brown, S., Norman, R. B., and Xu, X.: NAIRAS aircraft
28 radiation model development, dose climatology, and initial validation, *Space Weather*,
29 **11**, 603-635, doi:10.1002/swe.20100, 2013.
- 30 Mironova, I. A., Aplin, K. L., Arnold, F., Bazilevskaya, G. A., Harrison, R. G., Krivolutsky,
31 A. A., Nicoll, K. A., Rozanov, E. V., Turunen, E., Usoskin, I. G.: Energetic Particle
32 Influence on the Earth's Atmosphere, *Space Sci. Rev.*, **194**, 1-96, 2015.
- 33 Müller, R., and Crutzen, P. J.: A possible role of galactic cosmic rays in chlorine activation
34 during polar night, *J. Geophys. Res.*, **98**, 20483-20490, 1993.
- 35 Nicolet, M.: On the production of nitric oxide by cosmic rays in the mesosphere and
36 stratosphere, *Planet. Space Sci.*, **23**, 637-649, 1975.
- 37 Norman, R. B., Blattnig, S. R., De Angelis, G., Badavi, F. F., and Norbury, J. W.:
38 Deterministic pion and muon transport in Earth's atmosphere, *Adv. Space Res.*, **50**, 146-
39 155, 2012.
- 40 Norman, R. B., Slaba, T. C., and Blattnig, S. R.: An extension of HZETRN for cosmic ray
41 initiated electromagnetic cascades, *Adv. Space Res.*, **51**, 2251-2260, 2013.
- 42 O'Neill, P. M. : Badhwar-O'Neill 2010 galactic cosmic ray flux model – Revised, *IEEE*
43 *Trans. Nucl. Sci.*, **57**(6), 3148-3153, 2010.
- 44 Picone, J. M., Hedin, A. E., Drob, D. P., and Aikin, A. C.: NRLMSIS-00 empirical model of
45 the atmosphere: Statistical comparisons and scientific issues, *J. Geophys. Res.*,
46 **107**(A12), 1468, 10/1029/2002JA009430, 2002.
- 47 Porter, H. S., Jackman, C. H., and Green, A. E. S.: Efficiencies for production of atomic
48 nitrogen and oxygen by relativistic proton impact in air, *J. Chem. Phys.*, **65**, 154-167,
49 1976.

- 1 Rienecker, M. M., Suarez, M. J., Gelaro, R., Todling, R., Bacmeister, J., Liu, E., Bosilovich,
2 G., Schubert, S. D., Takacs, L., Kim, G.-K., Bloom, S., Chen, J., Collins, D., Conaty,
3 A., da Silva, A., Gu, W., Joiner, J., Koster, R. D., Lucchesi, R., Molod, A., Owens, T.,
4 Pawson, S., Pegion, P., Redder, C. R., Reichle, R., Robertson, F. R., Ruddick, A. G.,
5 Sienkiewicz, M., and Woollen, J.: MERRA: NASA's modern-era retrospective
6 analysis for research and applications, *J. Climate*, *24*, 3624–3648, doi:10.1175/JCLI-
7 D-11-00015.1, 2011.
- 8 Ruderman, M. A., and Chamberlain, J. W.: Origin of the sunspot modulation of ozone: Its
9 implications for stratospheric NO injection, *Planet. Space Sci.*, *23*, 247-268, 1975.
- 10 Sander, S. P., Abbatt, J., Barker, J. R., Burkholder, J. B., Friedl, R. R., Golden, D. M., Huie,
11 R. E., Kolb, C. E., Kurylo, M. J., Moortgat, G. K., Orkin, V. L., and Wine, P. H.:
12 Chemical kinetics and photochemical data for use in atmospheric studies, Evaluation
13 Number 17, JPL Publication 10-6., Pasadena, California, 2011.
- 14 Semeniuk, K., Fomichev, V. I., McConnell, J. C., Fu, C., Melo, S. M. L., and Usoskin, I. G.:
15 Middle atmosphere response to the solar cycle in irradiance and ionizing particle
16 precipitation, *Atmos. Chem. Phys.*, *11*, 5045-5077, 2011.
- 17 Slaba, T. C., Blattnig, S. R., Reddell, B., Bahadori, A., Norman, R. B., and Badavi, F. F.: Pion
18 and electromagnetic contribution to dose: Comparisons of HZETRN to Monte Carlo
19 results and ISS data, *Adv. Space Res.*, *52*, 62-78, 2013.
- 20 Smart, D. F. and Shea, M. A.: Geomagnetic cutoffs: A review for space dosimetry
21 calculations, *Adv. Space Res.*, *14*(10), 10,787-10,796, 1994.
- 22 Smart, D. F. and Shea, M. A.: A review of geomagnetic cutoff rigidities for earth-orbiting
23 spacecraft, *Adv. Space Res.*, *36*, 2012-2020, 2005.
- 24 Solomon, S., Rusch, D. W., Gerard, J.-C., Reid, G. C., and Crutzen, P. J.: The effect of
25 particle precipitation events on the neutral and ion chemistry of the middle
26 atmosphere, 2, Odd hydrogen, *Planet. Space Sci.*, *29*, 885-892, 1981.
- 27 Solomon, S., Kinnison, D., Bandoro, J., Garcia, R.: Simulations of Polar Ozone Depletion: An
28 Update, *J. Geophys. Res.*, *120*, 7958-7974, doi:10.1002/2015JD023365, 2015.
- 29 SPARC (Stratosphere-Troposphere Processes and their Role in Climate) Report on the
30 Lifetimes of Stratospheric Ozone-Depleting Substances, Their Replacements, and
31 Related Species: Ko, M. K. W., Newman, P. A., Reimann, S., and Strahan, S. E.
32 (Eds.), SPARC Report No. 6., WCRP-15/2013, [Available at [http://www.sparc-
33 climate.org/publications/sparc-reports/sparc-report-no6/](http://www.sparc-climate.org/publications/sparc-reports/sparc-report-no6/)], SPARC Office, Zurich,
34 Switzerland, 2013.
- 35 Spivakovsky, C. M., Logan, J. A., Montzka, S. A., Balkanski, Y. J., Foreman-Fowler, M.,
36 Jones, D. B. A., Horowitz, L. W., Fusco, A. C., Brenninkmeijer, C. A. M., Prather, M.
37 J., Wofsy, S. C., and McElroy, M. B.: Three-dimensional climatological distribution of
38 tropospheric OH: Update and evaluation, *J. Geophys. Res.*, *105*, 8931-8980,
39 doi:10.1029/1999JD901006, 2000.
- 40 Strahan, S. E., Duncan, B. N., and Hoor, P.: Observationally derived transport diagnostics for
41 the lowermost stratosphere and their application to the GMI chemistry and transport
42 model, *Atmos. Chem. Phys.*, *7*, 2435–2445, doi:10.5194/acp-7-2435-2007, 2007.
- 43 Strode, S.A., Rodriguez, J. M., Logan, J. A., Cooper, O. R., Witte, J. C., Lamsal, L. N.,
44 Damon, M., Van Aartsen, B., Steenrod, S. D., and Strahan, S. E.: Trends and
45 variability in surface ozone over the United States, *J. Geophys. Res. Atmos.* *120*, 9020-
46 9042, doi:10.1002/2014JD022784, 2015.
- 47 Thorne, R. M.: The importance of energetic particle precipitation on the chemical
48 composition of the middle atmosphere, *Pure Appl. Geophys.*, *118*, 128-151, 1980.

- 1 Usoskin, I. G., Kovaltsov, G. A., and Mironova, I. A.; Cosmic ray induced ionization model
2 CRAC:CR11; An extension to the upper atmosphere, *J. Geophys. Res.*, *115*, D10302,
3 doi:10.1029/2009JD013142, 2010.
- 4 Vitt, F. M., and Jackman, C. H.: A comparison of sources of odd nitrogen production from
5 1974 through 1993 in the Earth's middle atmosphere as calculated using a two-
6 dimensional model, *J. Geophys. Res.*, *101*, 6729-6739, 1996.
- 7 Vitt, F. M., Armstrong, T. P., Cravens, T. E., Dreschhoff, G. A. M., Jackman, C. H., and
8 Laird, C. M.: Computed contributions to odd nitrogen concentrations in the Earth's
9 polar middle atmosphere by energetic charged particles, *J. Atmos. Solar-Terr. Phys.*,
10 *62*, 669-683, 2000.
- 11 Warneck, P.: Cosmic radiation as a source of odd nitrogen in the stratosphere, *J. Geophys.*
12 *Res.*, *77*, 6589-6591, 1972.
- 13 Wegner, T., Kinnison, D. E., Garcia, R. R., and Solomon, S.: Simulation of polar
14 stratospheric clouds in the specified dynamics version of the whole atmosphere
15 community climate model, *J. Geophys. Res. Atmos.*, *118*, 4991–5002,
16 doi:10.1002/jgrd.50415, 2013.
- 17 WMO (World Meteorological Organization): Scientific Assessment of Ozone Depletion:
18 2014, Global Ozone Research and Monitoring Project-Report No. 55, Geneva,
19 Switzerland, 2014.

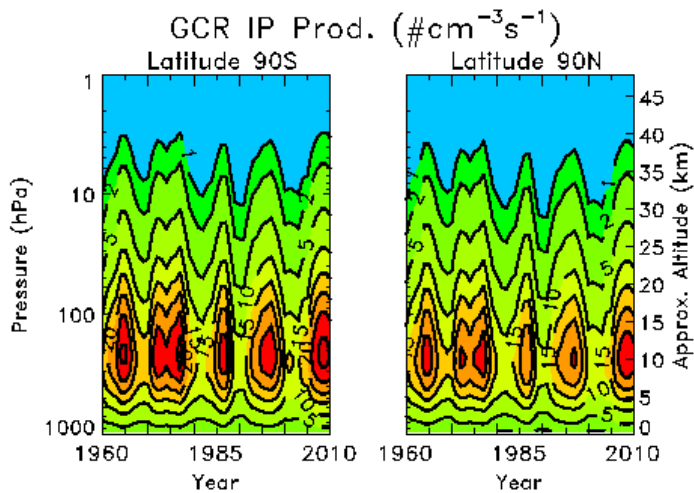
<i>Simulation Designation</i>	<i>Model</i>	<i>Time Period (Years)</i>	<i>Include GCRs</i>	<i>Other Information</i>
<i>Base_SD-W</i>	SD-WACCM	2000-2009	No	Interannual MERRA Transport No Sulfate Aerosol (SA) Variation No Solar Cycle (SC) Photon Flux (PF) Variation
<i>GCR_SD-W</i>	SD-WACCM	2000-2009	Yes, Interannually Varying	Interannual MERRA Transport No SA Var., No SC PF Var.
<i>A_Base_GSFC</i>	GSFC 2-D	1960-2010	No	Climatological Averaged Transport No SA Var., No SC PF Var.
<i>B_Base_GSFC</i>	GSFC 2-D	1960-2010	No	Interannual Transport No SA Var., No SC PF Var.
<i>C_Base_GSFC</i>	GSFC 2-D	1960-2010	No	Climatological Averaged Transport SA Var., No SC PF Var.
<i>D_Base_GSFC</i>	GSFC 2-D	1960-2010	No	Climatological Averaged Transport No SA Var., SC PF Var.
<i>E_Base_GSFC</i>	GSFC 2-D	1960-2010	No	Interannual Transport SA Var., SC PF Var.
<i>A1_GCR_GSFC</i>	GSFC 2-D	1960-2010	Yes, Mean of Values	Climatological Averaged Transport No SA Var., No SC PF Var.
<i>A2_GCR_GSFC</i>	GSFC 2-D	1960-2010	Yes, Interannually Varying	Climatological Averaged Transport No SA Var., No SC PF Var.
<i>B1_GCR_GSFC</i>	GSFC 2-D	1960-2010	Yes, Mean of Values	Interannual Transport No SA Var., No SC PF Var.
<i>B2_GCR_GSFC</i>	GSFC 2-D	1960-2010	Yes, Interannually Varying	Interannual Transport No SA Var., No SC PF Var.
<i>C_GCR_GSFC</i>	GSFC 2-D	1960-2010	Yes, Mean of Values	Climatological Averaged Transport SA Var., No SC PF Var.
<i>D_GCR_GSFC</i>	GSFC 2-D	1960-2010	Yes, Mean of Values	Climatological Averaged Transport No SA Var., SC PF Var.
<i>E_GCR_GSFC</i>	GSFC 2-D	1960-2010	Yes, Interannually Varying	Interannual Transport SA Var., SC PF Var.



12 Figure 1. NAIAS model computed GCR annual average ionization rates for years 2002
 13 (left) and 2009 (right). Contour intervals are 1, 2, 5, 10, 15, 20, 25, and 30 ($\text{#cm}^{-3} \text{s}^{-1}$).

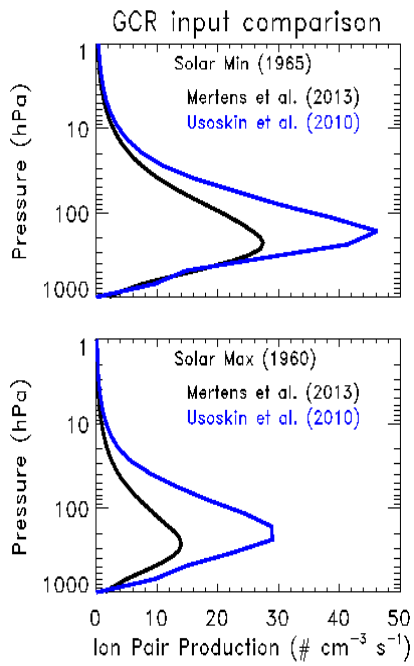
14

15



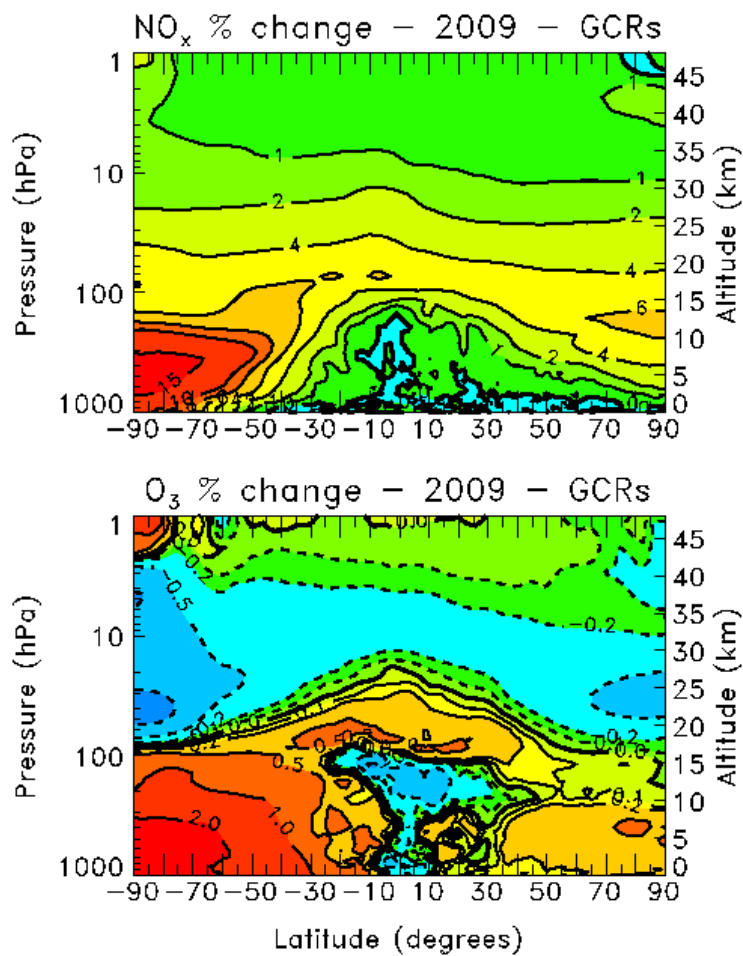
16

17 Figure 2. NAIAS model computed galactic cosmic ray annual average ionization rates at
 18 90°S (left) and 90°N (right) over the time period 1960-2010. Contour intervals are 1, 2, 5, 10,
 19 15, 20, 25, and 30 ($\text{#cm}^{-3} \text{s}^{-1}$).



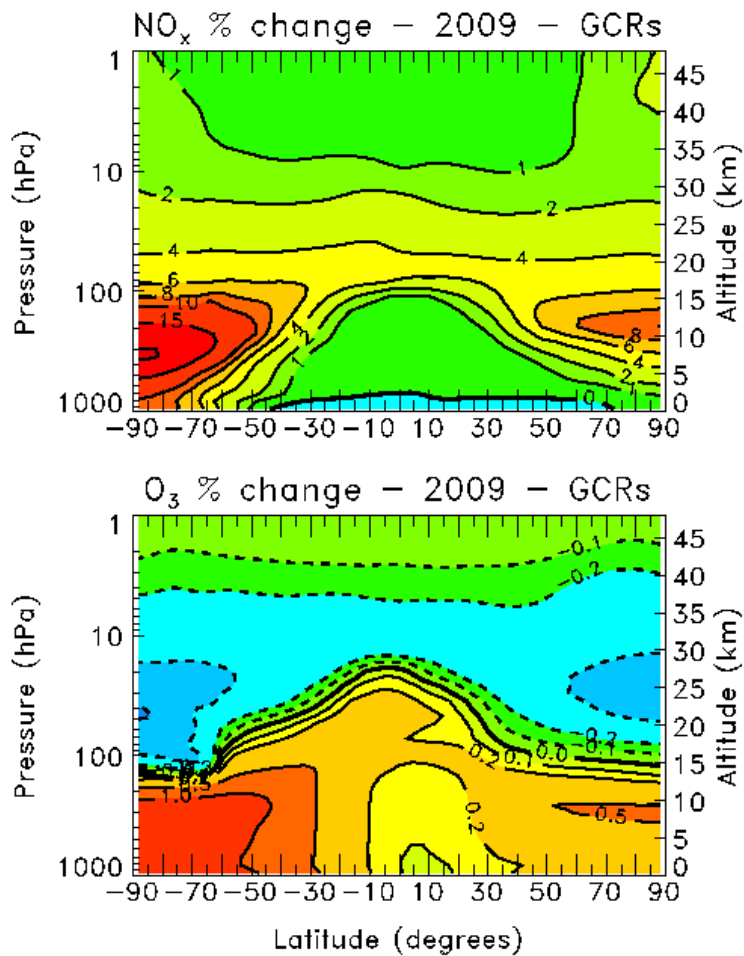
1

2 Figure 3. NAIRAS model computed galactic cosmic ray annual average ionization rates
 3 (Mertens et al., 2013) compared to those given in Usoskin et al. (2010) for solar minimum
 4 (1965, top plot) and solar maximum (1960, bottom plot).



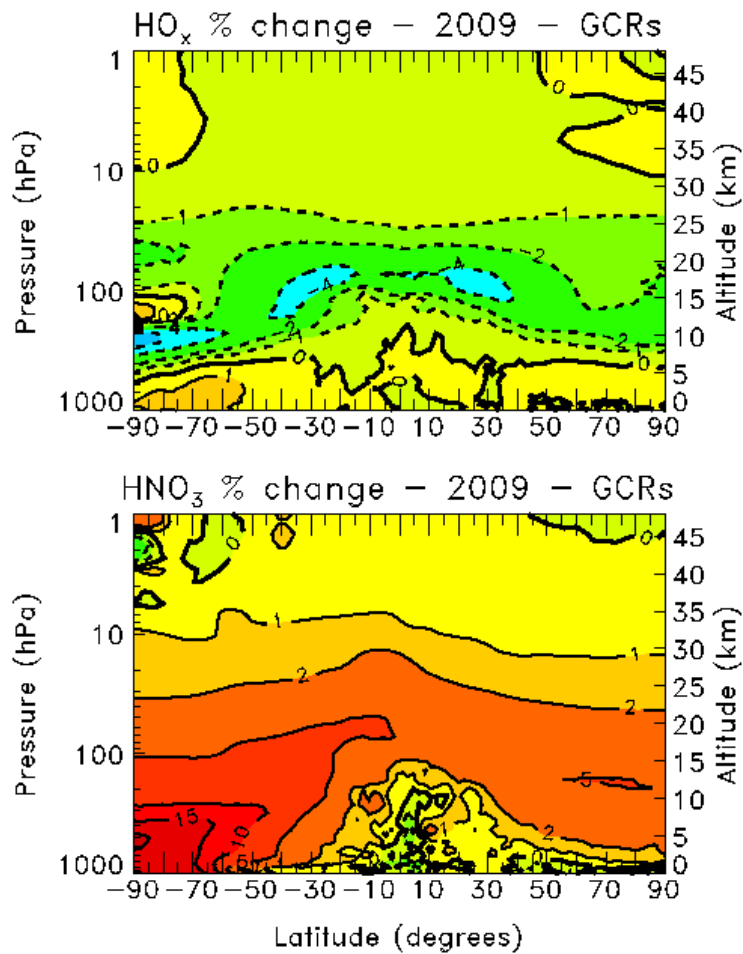
1

2 Figure 4. Annual average percentage change for year 2009 in zonal mean NO_x (top) and
 3 ozone (bottom) due to GCRs in the SD-WACCM (simulation *Base_SD_W* compared to
 4 *GCR_SD_W*). The contour intervals for the NO_x changes are 0, 1, 2, 4, 6, 8, 10, and 15%.
 5 The contour intervals for the ozone changes are -1, -.5, -.2, -.1, 0, .1, .2, .5, 1, and 2%.



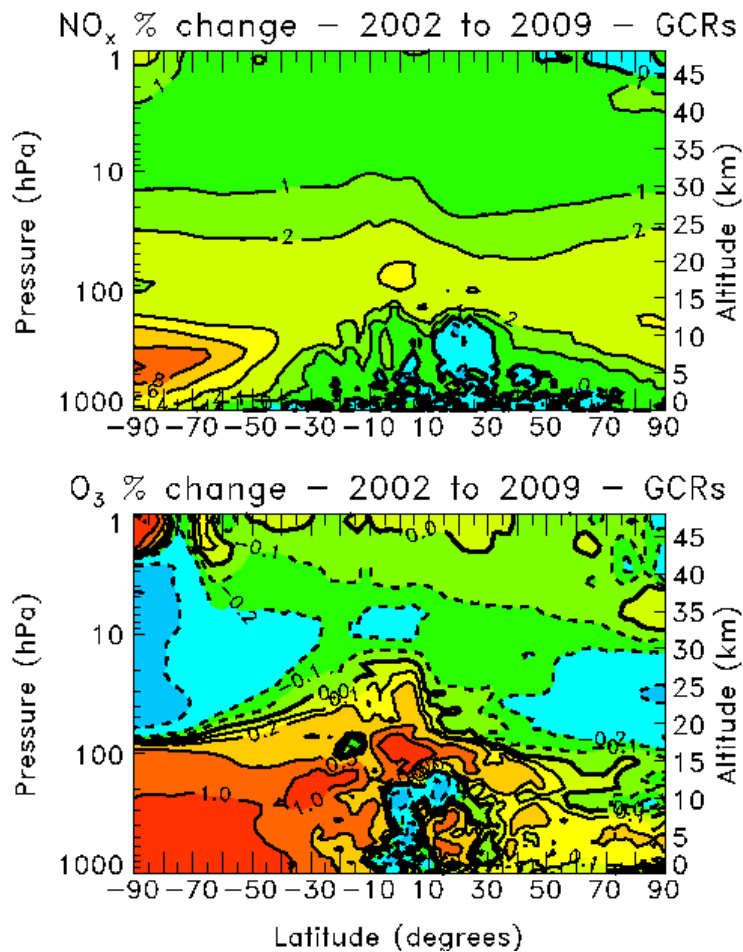
1

2 Figure 5. Annual average percentage change for year 2009 in zonal mean NO_x (top) and
 3 ozone (bottom) due to GCRs in the GSFC 2-D model (simulation *B2_GCR_GSFC* compared
 4 to *B_Base_GSFC*). The contour intervals for the NO_x changes are 0, 1, 2, 4, 6, 8, 10, 15, and
 5 20%. The contour intervals for the ozone changes are -1, -.5, -.2, -.1, 0, .1, .2, .5, and 1%.



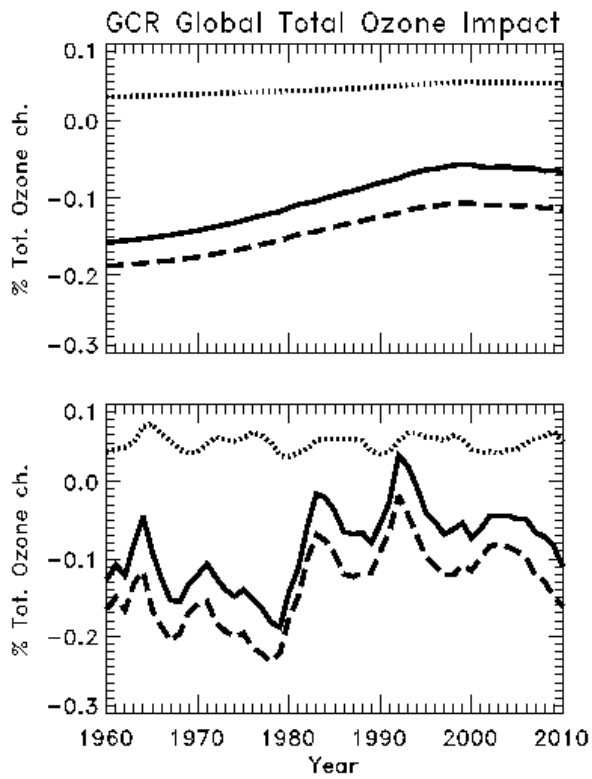
1

2 Figure 6. Annual average percentage change for year 2009 in zonal mean HO_x (top) and
 3 HNO₃ (bottom) due to GCRs in the SD-WACCM (simulation *Base_SD_W* compared to
 4 *GCR_SD_W*). The contour intervals for the HO_x changes are -6, -4, -2, -1, 0, and 1%. The
 5 contour intervals for the HNO₃ are -1, 0, 1, 2, 5, 10, 15, and 20%.



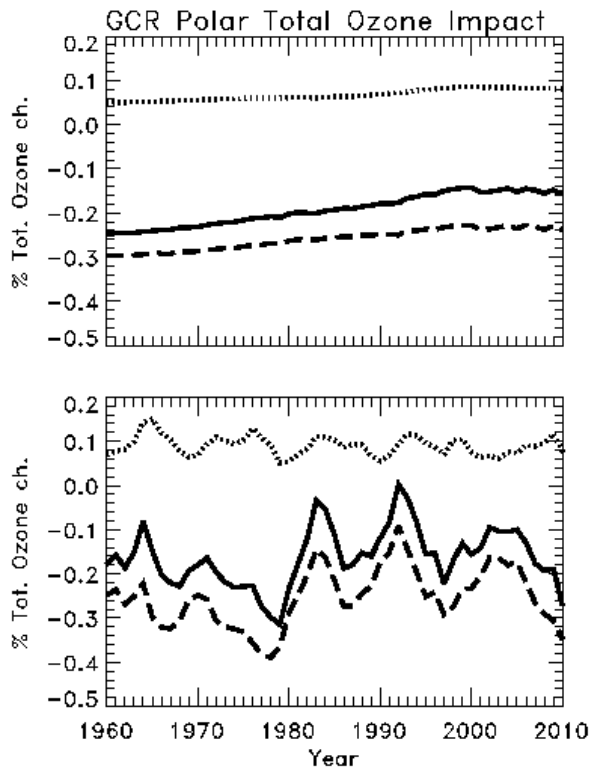
1
2

3 Figure 7. Annual average percentage change from year 2002 (solar maximum) to 2009 (solar
4 minimum) in zonal mean NO_x (top) and ozone (bottom) in the SD-WACCM. Simulations
5 *GCR_SD-W* and *Base_SD-W* were used for this comparison. The annual average percentage
6 change from GCRs was computed for years 2002 and 2009 separately and then differenced
7 from each other. The contour intervals for the NO_x changes are 0, 1, 2, 4, 6, 8, and 10%. The
8 contour intervals for the ozone changes are -1, -.5, -.2, -.1, 0, .1, .2, .5, and 1%.



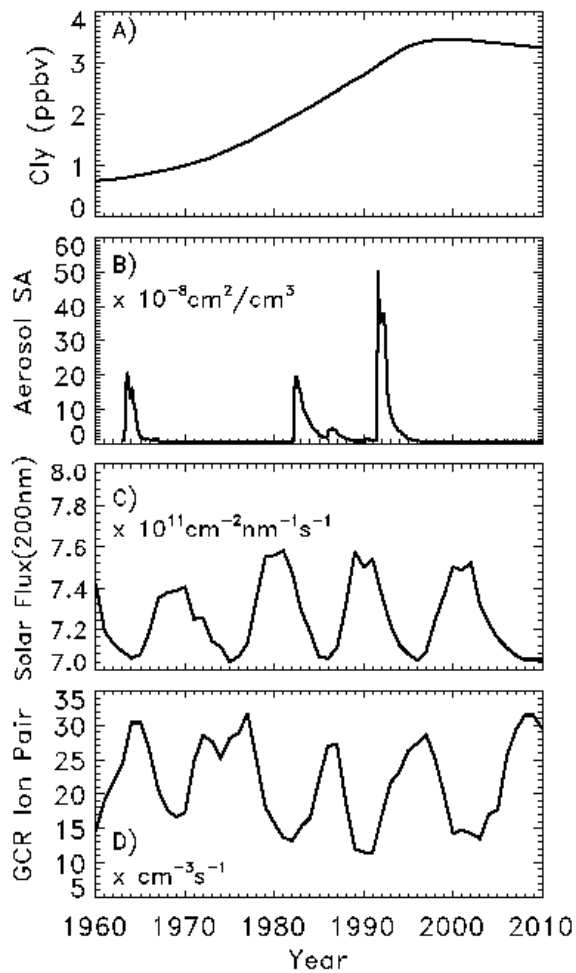
1

2 Figure 8. GSFC 2-D model GCR-computed tropospheric column (dotted black), stratospheric
 3 column (dashed black), and total (solid black) AAGTO impacts over the 1960-2010 time
 4 period. The top plot shows the comparison of simulation *AI_GCR_GSFC* to *A_Base_GSFC*.
 5 The bottom plot shows the comparison of simulation *E_GCR_GSFC* to *E_Base_GSFC*.



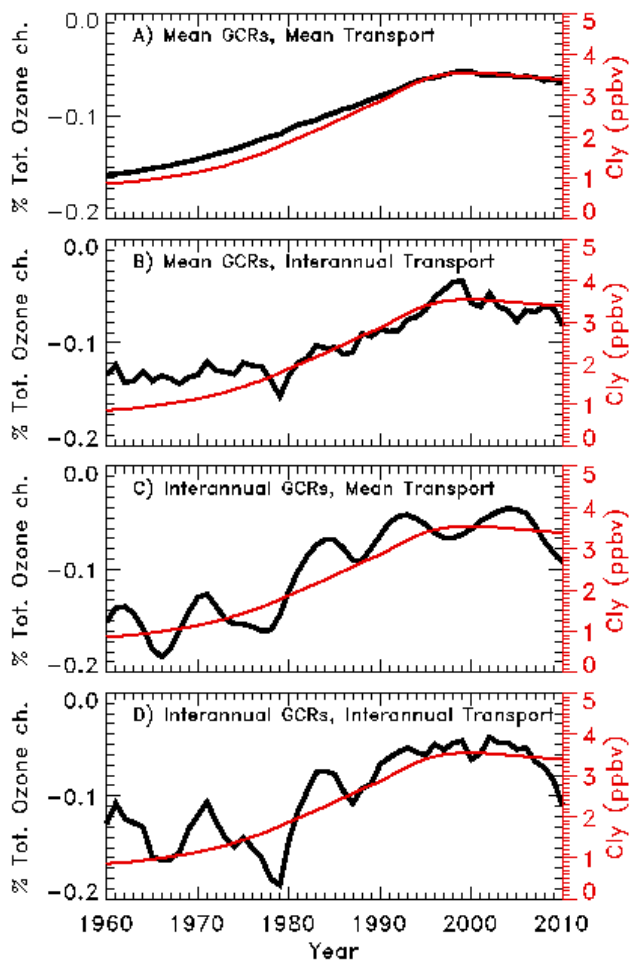
1

2 Figure 9. GSFC 2-D model GCR-computed impacts of annual average polar total ozone
 3 (AAPTO) between 1000 and 100 hPa (dotted black), between 100 and 1 hPa (dashed black),
 4 and for the entire troposphere and stratosphere, 1000 to 1 hPa, (solid black) over the 1960-
 5 2010 time period. The top plot shows the comparison of simulation A1_GCR_GSFC to
 6 A_Base_GSFC. The bottom plot shows the comparison of simulation E_GCR_GSFC to
 7 E_Base_GSFC.



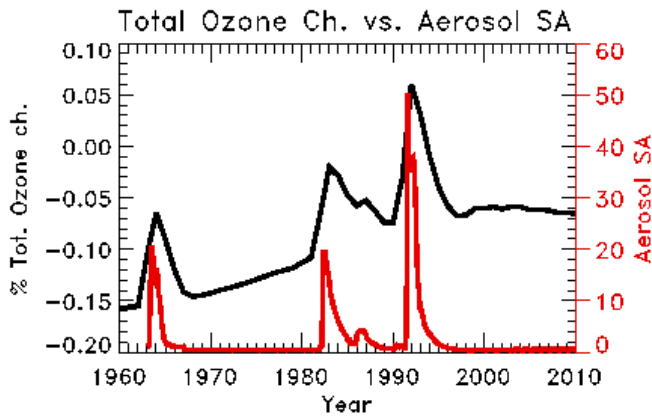
1

2 Figure 10. Forcing used in the GSFC 2-D model over the 1960-2010 time period. These
 3 include: A) Background Total Chlorine (Cl_y , in ppbv); B) Aerosol Surface Area (SA) at 50
 4 hPa and the Equator in $10^{-8} \text{ cm}^2/\text{cm}^3$; C) Solar Flux at 200 nm in $10^{11} \text{ cm}^{-2} \text{ nm}^{-1} \text{ s}^{-1}$; and D)
 5 GCR Ion Pair Production at 200 hPa and 90°S in $\text{cm}^{-3} \text{ s}^{-1}$.



1

2 Figure 11. GSFC 2-D model GCR-computed AAGTO impacts (black lines) over the 1960-
 3 2010 time period. The Cl_y levels are also shown (red lines). The GSFC 2-D model
 4 comparisons include: A) Mean GCRs, Mean Transport (simulation *A1_GCR_GSFC*
 5 compared to *A_Base_GSFC*); B) Mean GCRs, Interannual Transport (simulation
 6 *B1_GCR_GSFC* compared to *B_Base_GSFC*); C) Interannual GCRs, Mean Transport
 7 (simulation *A2_GCR_GSFC* compared to *A_Base_GSFC*); and D) Interannual GCRs,
 8 Interannual Transport (simulation *B2_GCR_GSFC* compared to *B_Base_GSFC*).

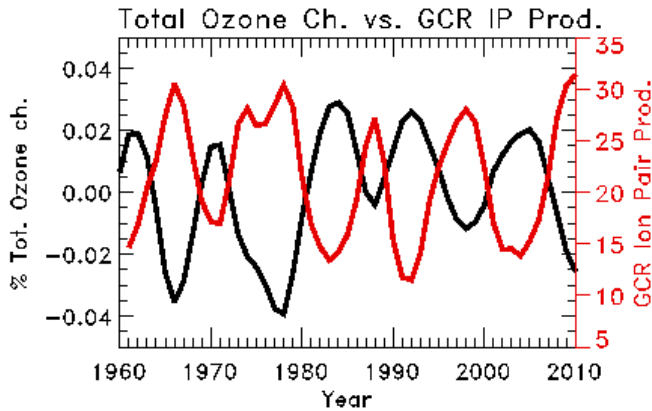


1

2 Figure 12. GSFC 2-D model GCR-computed AAGTO impacts (black line) over the 1960-
 3 2010 time period (simulation *C_GCR_GSFC* compared to *C_Base_GSFC*). The Aerosol
 4 Surface Area (SA) at 50 hPa and the Equator is also shown (red lines), given in $10^{-8} \text{ cm}^2/\text{cm}^3$.

5

6



7

8 Figure 13. GSFC 2-D model GCR-computed AAGTO change (black line) over the 1960-
 9 2010 time period caused by the interannual GCR variation. The global total ozone change
 10 shown in Figure 11C is differenced from that shown in Figure 11A. A two-year boxcar
 11 (running) average of the GCR Ion Pair Production (in $\text{cm}^{-3}\text{s}^{-1}$) at 200 hPa and 90°S with a
 12 one-year lag is also shown (red line).